



ELSEVIER

Physica D 116 (1998) 342–354

PHYSICA D

Deterministic Brownian motion in the hypermeander of spiral waves

V.N. Biktashev^{a,b,*}, A.V. Holden^b

^a *Institute for Mathematical Problems in Biology, Pushchino, Moscow Region, 142292, Russian Federation*

^b *Department of Physiology, University of Leeds, Leeds LS2 9JT, UK*

Received 10 March 1997; received in revised form 7 October 1997; accepted 17 November 1997

Communicated by C.K.R.T. Jones

Abstract

We explain the phenomenon of hypermeander of spiral waves, observed in numerical experiments with various models of excitable media, as a chaotic attractor in the quotient system with respect to the Euclidean group. Such an attractor should lead to a motion of the spiral wave tip analogous to that of a Brownian particle, with mean square of displacement of the tip growing linearly at large times. This prediction is confirmed by numerical experiments with hypermeandering spiral waves. Copyright © 1998 Elsevier Science B.V.

Keywords: Excitable media; Spiral wave; Skew product; Deterministic diffusion

1. Introduction

In [1] we have shown how the Euclidean symmetry group of the plane can be exploited to split the analysis of spiral wave dynamics into motion in a reduced non-symmetric ‘quotient’ dynamic system, and drift along the group. For a reaction–diffusion system

$$\partial_t u = \mathbf{D} \nabla^2 u + f(u) \quad (1)$$

with $u(\mathbf{r}, t) = (u_1, u_2, \dots) \in \mathbb{R}^l$, $l \geq 2$, $\mathbf{r} = (x, y) \in \mathbb{R}^2$, the reduced dynamic system is the system of l PDEs and three finite equations,

$$\begin{aligned} \partial_t v &= \mathbf{D} \nabla^2 v + f(v) - (\mathbf{c}, \nabla) v - \omega \partial_\theta v, \\ 0 &= g_1(v(\mathbf{0}, t)), \quad 0 = g_2(v(\mathbf{0}, t)), \quad 0 = \partial_x g_3(v(\mathbf{0}, t)), \end{aligned} \quad (2)$$

for $l + 3$ dynamic variables (v, \mathbf{c}, ω) , $v(\mathbf{r}, t) \in \mathbb{R}^l$, $\mathbf{c}(t) = (c_x(t), c_y(t)) \in \mathbb{R}^2$, $\omega(t) \in \mathbb{R}$, where the g_j are real functions and $\partial_\theta = y \partial_x - x \partial_y$. Drift along the group is described by equations

* Corresponding author. Address: Department of Physiology, University of Leeds, Leeds LS2 9JT, UK.

$$\partial_t \Theta = \omega(t), \quad (3)$$

$$\partial_t R = c(t) \exp(i\Theta), \quad (4)$$

where $c = c_x + ic_y$, and $R = X + iY \in \mathbb{C}$ and $\Theta \in \mathbb{R}$ are coordinates along the Euclidean group¹ $\mathbf{SE}(2)$, the displacement vector and rotation angle, respectively.

The mathematical idea of this operation is reduction of the dynamics onto the manifold of group orbits, which is a standard technique for finite-dimensional systems [2]. Here we used it for PDEs, and parametrised the orbit manifold by a manifold lying in the phase space transversal to the orbits. In this particular case, this splitting into two parts has a simple visual interpretation: the first of Eqs. (2) is the reaction–diffusion system in a moving frame of reference, while the next two say that this frame is chosen so that a specific point of the spiral wave, naturally associated with the spiral wave tip, is always located at the origin and the last equation fixes relative orientation of the spiral tip and of the frame of reference. A typical choice of functions g_j is:

$$g_1(v) \equiv v_1 - v_{10}, \quad g_2(v) \equiv v_2 - v_{20}, \quad g_3(v) \equiv v_1, \quad (5)$$

with some constants v_{10} , v_{20} , which correspond to the definition of the tip as intersection of two isolines, in this example of components 1 and 2, and orientation of the tip defined as that of the gradient of the first component. Hence, the equations along the group (3),(4) are interpreted as motion equations of the spiral tip, with R being its complex coordinate and Θ its orientation.

In [1] we have shown that, in particular, this approach provides a simple derivation of Barkley's [3–5] model system for the bifurcation from simple to compound rotation, recently studied rigorously by Wulff [6] in the original system with symmetry. In our approach, this corresponds simply to the standard Andronov–Hopf bifurcation in the quotient system (2).

The compound two-periodic rotation of spiral wave is not the only type of meander pattern, and more complicated patterns have been reported in literature [7–9]; Winfree [7] has called this behaviour ‘hypermeander’. A specific feature of hypermeander is that the spiral tip trajectory appears complicated, and not compact, i.e. it goes outside any prescribed region – or, at least, has a much larger excursion than the bi-periodic meander of the same model with similar values of parameters.

In this paper we discuss the hypothesis put forward in [1,3,5,9] that hypermeander is related to some chaotic behaviour, and more specifically, a chaotic attractor in the quotient system (2). We show that in this case the spiral tip trajectory is not compact, but walks around the plane, and at large time this walk is analogous to Brownian motion. This prediction is consistent with numerical experiments.

2. Deterministic Brownian motion

2.1. Mathematical background

The classical theory of Brownian motion considers it as a stochastic process, i.e. as a motion driven by a random force that results from the superposition of a large number of independent collisions. Deterministic chaos has similar effects to a stochastic process, and motion driven by a force depending on a single low-dimensional chaotic process can exhibit properties similar to those of stochastic Brownian motion, e.g. mean walking distance $\sim t^{1/2}$, and is then called deterministic Brownian motion or deterministic diffusion. The well-studied classes of such processes, starting from the work [10], are chaotic and periodic iterated maps; there the possibility of macroscopic ‘diffusion’

¹ We consider only the subgroup of orientation-preserving motions.

motion is provided by a non-compact discrete group of translations. Here we deal with a continuous symmetry group and continuous time, and will use a continuous version of corresponding statements:

Theorem 1. Let a semi-flow F^t in a Banach space \mathcal{B}

$$u \mapsto F^t(u), \quad u \in \mathcal{B}, \quad t \geq 0$$

be ergodic with an invariant measure μ , $\int d\mu = 1$. Suppose a function $V(u) : \mathcal{B} \rightarrow \mathbb{R}$ has a zero mean value in μ ,

$$V_0 \triangleq \int V(u) d\mu(u) = 0,$$

and its autocorrelation function

$$K(\tau) \triangleq \int V(u) V(F^{|\tau|}(u)) d\mu(u) \tag{6}$$

quickly decays; more precisely,

$$K_0 \triangleq \int_{-\infty}^{+\infty} K(\tau) d\tau < \infty. \tag{7}$$

Consider a point with coordinate $q \in \mathbb{R}$ moving with the velocity V ,

$$\partial q(t, u) / \partial t = V(F^t(u)). \tag{8}$$

Then the mean squared displacement of the point in a given time interval t ,

$$I(t, u) \triangleq \lim_{T \rightarrow +\infty} \frac{1}{T} \int_0^T (q(\tau + t, u) - q(\tau, u))^2 d\tau,$$

grows linearly at large t ,

$$I(t, u) = K_0 t + o(t), \quad t \rightarrow +\infty, \tag{9}$$

for almost all u with respect to μ .

If a stronger condition on the autocorrelation function is fulfilled,

$$-\frac{1}{2} K_1 \triangleq \int_0^\infty d\tau \int_\tau^\infty K(\xi) d\xi < \infty, \tag{10}$$

then this estimation can be strengthened:

$$I(t, u) = K_0 t + K_1 + o(1), \quad t \rightarrow +\infty. \tag{11}$$

We did not find a proof of this statement in literature, and so we present it in Appendix A.

We assume that the invariant measure, ergodicity and quickly decaying correlation functions are consequences of a chaotic attractor of the semi-flow F^t , though detailed specification of suitable attractors would lead us away from the main subject.

Naturally, in case of non-zero V_0 , the mean square of the displacement grows as $(V_0 t)^2$, i.e. there is a directed drift with velocity V_0 rather than Brownian walk. However, it is easy to see that if other conditions of Theorem 1 are fulfilled, in the frame of reference moving with velocity V_0 we shall observe Brownian walk again. In other words, in general case there is a superposition of the directed and Brownian motions.

2.2. Example: Deterministic diffusion in \mathbb{R}^1

Theorem 1 can be directly applied to the case of chaos-driven walk along a straight line, as recently described by Couillet and Emilsson [11]. This is Ising–Bloch wall dynamics in a modified complex Ginzburg–Landau equation:

$$\partial_t u = \lambda u - \beta |u|^2 u + \alpha \partial_x^2 u + \gamma \bar{u} = f(u) + \alpha \partial_x^2 u \quad (12)$$

for $\alpha, \beta, \lambda, u(x, t) \in \mathbb{C}$ and $\gamma, x, t \in \mathbb{R}$.

At some parameter values, there are two stable equilibria $u_{1,2}$ in the spatially homogeneous system $\partial_t u = f(u)$, and solutions are considered which asymptotically approach one equilibrium at $x \rightarrow +\infty$ and the other at $x \rightarrow -\infty$. This equation is invariant under the group of translations along the x -axis. Reduction by this group, in the same style as we did it for reaction–diffusion system (1) and Euclidean group **SE**(2), yields the quotient system

$$\partial_t v = f(v) + \alpha \partial_x^2 v - c \partial_x v, \quad 0 = g(v(0, t)) \quad (13)$$

for dynamic variables v and c , where

$$v(x, t) = u(x - X(t), t), \quad (14)$$

and $g(v) \in \mathbb{R}$ could be chosen, say $\text{Re}(v) - v_0$ or $\text{Im}(v) - v_0$. X can be considered as the wall coordinate, then drift along the group is the wall motion, and is described simply by

$$dX/dt = c(t). \quad (15)$$

Couillet and Emilsson [11] simulated the dynamics of the wall solutions and analysed them in terms of the quantity $M(t)$ defined as

$$M(t) = \int |\partial_x u(x, t)|^2 dx, \quad (16)$$

which is invariant under the group, i.e. is a functional of the quotient system (13). At some parameter values, they have found that time-delay plots $M(t)$ vs. $M(t + \tau)$ showed pictures typical for chaotic attractors. Assuming that this implies invariant measure, ergodicity and decaying correlation functions, we can apply Theorem 1, by identifying the semi-flow generated by (13) with F^t of Theorem 1, X with q and c with V . In accordance with the statement of Theorem 1, in the case of even distribution of the velocity, which took place in a region of parameters, Couillet and Emilsson observed ‘diffusive’ motion with a root mean squared displacement that scaled as $t^{1/2}$. In the case of non-even distribution which happened in between the ‘diffusive’ parameter range, the root mean squared displacement scaled as t , which might correspond to the superposition of directed and Brownian motion.

2.3. Application to hypermeander

For our present case of diffusion along **SE**(2), application of Theorem 1 is not so simple, as the group manifold not only is not a straight line (it is three-dimensional), but is ‘curved’, due to the non-commutativity of **SE**(2).

Formally, this is represented by the fact that Eqs. (3) and (4) neither have a simple form (8), nor can be reduced to one. So, the straightforward identification of q of Theorem 1 with Euclidean-group coordinates X, Y and Θ , and the semi-flow F^t with that generated by the dynamical system (2), do not work. In this case, the tip coordinates $R(t) = X(t) + iY(t)$ are determined via two indefinite integrals, the first to find $\Theta(t)$ from $\omega(t)$, and the second to find $R(t)$ from $c(t)$ and $\Theta(t)$. Correspondingly, Theorem 1 should be applied twice, to each of the indefinite integrals, and the second application does not succeed due to the possibility of correlation between $\Theta(t)$ and $c(t)$,

as they come from the same dynamic system. Conceivably, this is not just a technical difficulty, but reflects the essence of the problem, as it is seen from the following alternative viewpoint.

Let us reduce (1) by the subgroup of translations only. The quotient system is

$$\partial_t w = \mathbf{D}\nabla^2 w + f(w) - (\mathbf{C}, \nabla)w, \quad w_1(\mathbf{0}, t) = u_{10}, \quad w_2(\mathbf{0}, t) = u_{20} \quad (17)$$

for dynamic variables w ,

$$w(x, y, t) = u(x - X(t), y - Y(t), t), \quad (18)$$

and $\mathbf{C} = (C_x, C_y)$, and motion along the group is motion of the tip,

$$\partial_t X = C_x, \quad \partial_t Y = C_y. \quad (19)$$

Note that the ‘semi-reduced system’ (17) is still invariant under the subgroup of rotations of the Euclidean group, $\mathbf{SO}(2) \subset \mathbf{SE}(2)$, represented as simultaneous rotations of vector \mathbf{C} and arguments of w .² The subgroup of translations is commutative, the dynamics of X and Y are separated, and we can identify q of Theorem 1 with X and Y , V with C_x and C_y , and F^t with the semi-flow generated by (17). As the semi-reduced system is still invariant under $\mathcal{G} = \mathbf{SO}(2)$, its maximal attractor must be invariant under this group, but can be split into invariant subsets, each invariant under a subgroup $\mathcal{S} \subset \mathcal{G}$. This subgroup could be either $\mathbf{SO}(2)$ itself, in which case the only invariant subset coincides with the whole maximal attractor, or \mathbf{Z}_m , $m \in \mathbb{N}$ or the trivial group, and then there are many invariant subsets. Let us consider all these cases:

1. If \mathcal{S} is $\mathbf{SO}(2)$ or \mathbf{Z}_m , $m > 1$, then the mean value of \mathbf{C} vanishes, as required by Theorem 1, and the tip undergoes Brownian motion in the plane. As the motion is in both the x and y directions, the mean squared walking distance is

$$\begin{aligned} I(t, u) &= \lim_{T \rightarrow +\infty} \frac{1}{T} \int_0^T [(X(\tau + t, u) - X(\tau, u))^2 + (Y(\tau + t, u) - Y(\tau, u))^2] d\tau \\ &= 2K_0 t + 2K_1 + o(1), \quad t \rightarrow +\infty, \end{aligned} \quad (20)$$

where K_0 and K_1 are parameters of correlation function of each of the velocities C_x and C_y . This corresponds to diffusion coefficient $K_0/2$.

2. Alternatively, if \mathcal{S} is the trivial group, then the mean value of the tip velocity $C_0 = \int \mathbf{C} d\mu_1$ is generically non-zero, if averaged over an ergodic component of measure μ_1 , corresponding to an invariant subset of the attractor. In this case, there will be a superposition of directed drift with the velocity $|C_0|$ and direction depending on the particular trajectory at the maximal attractor, and a Brownian walk.

In a particular system, either case may take place. In an analogous problem, that of periodic solutions in systems with finite symmetry groups, it is known that symmetry subgroup of a periodic solution is a robust property, in the sense that it changes only at bifurcation points [12]. Here we deal with continuous groups and chaotic attractors, and so the question is more complicated. As pointed out by Mantel and Barkley [13], in the case of quasi-periodic behaviour in the quotient system, there is directed drift and hence splitting of the attractor in the semi-reduced system for a set of parameters which is everywhere dense, as well as the set of non-split attractors. For the chaotic case considered here, results of Jones and Parry [14] can be applied. Namely, Theorem 5 of [14] claims, in certain assumptions, that if the quotient system is uniquely ergodic, the full system is also uniquely ergodic, for ‘almost

² Equivalently, the semi-reduced system can be obtained by combining (2) and (3), and identifying $C = C_x + iC_y$ with $c \exp(i\theta)$ so that (19) corresponds to (4). The group $\mathbf{SO}(2)$ is represented in the semi-reduced system (2)+(3) by shifts in θ .

all' parameters. In our case, assuming unique ergodicity in (2) and applied to the group $\mathbf{SO}(2)$, this theorem means that a non-split attractor in (17) is the typical case, while a split attractor is the case of measure zero. However, this does not exclude the possibility of both the cases being everywhere dense.

Note that the trajectory of the tip would be erratic in either case, and in practice they may be indistinguishable, especially if the hypermeander diffusion coefficient $K_0/2$ is large and the mean velocity C_0 is small, or experimental noise or round-off errors are significant.

To sum up, we see that if the quotient system of the spiral wave has a chaotic attractor, then the trajectory of the tip will not only look complicated, but also be non-compact. The long-time asymptotics of tip motion would be either a Brownian motion or a superposition of the Brownian motion and a directed drift, with direction depending on initial conditions and perhaps slowly varying due to experimental noise or round-off errors.

In either case, a chaotic attractor in the quotient system may explain the corresponding feature of the hypermeandering spiral waves.

3. Numerical illustration

The prediction of quasi-Brownian behaviour made in the previous section could be verified within the limits of the model system, in the style of [9] or [13]. This, however, would be essentially a numerical check of rigorously proved statements, and so it is more interesting to observe this type of behaviour in a particular reaction–diffusion system. There are a few papers in which hypermeandering spiral waves were reported; not all of them were we able to reproduce. So, the cubic FitzHugh–Nagumo model with parameters reported in [7] as providing a hypermeander, did show a rather complicated behaviour – however, in our experiments this complicated behaviour only lasted a few dozens of spiral revolutions, whereafter standard flower-like meander established. The Oregonator model with parameters described in [8] showed complicated and obviously not flower-like tip trajectory. However, that trajectory remained compact for the longest timescales we followed it (up to 2.5×10^3 t.u.), which, apparently, means that the quotient system had complicated but not chaotic dynamics. This is consistent with observations of Plesser and Müller [15] of up to four-periodic motions and no chaos in Oregonator spiral waves.

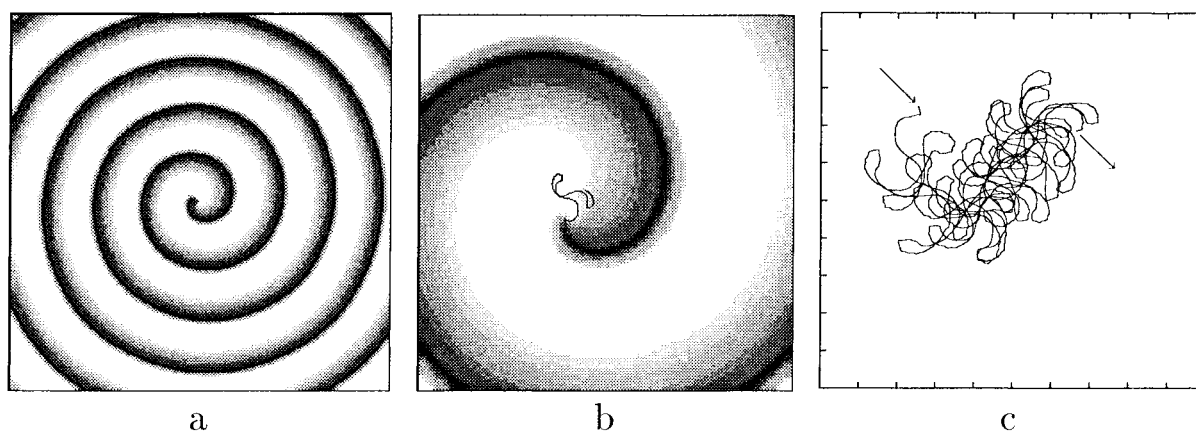


Fig. 1. (a) Spiral wave in the medium 80×80 s.u. large. Darkness of shading shows sum of the values of activator variable u_1 and inhibitor variable u_2 . (b) Same, in the medium 20×20 s.u. The black line is a piece of trajectory of the tip. (c) Piece of the tip trajectory during 40 t.u.; arrows show begin and end of the piece, size of the square is 10×10 s.u., cut from the medium 80×80 s.u.

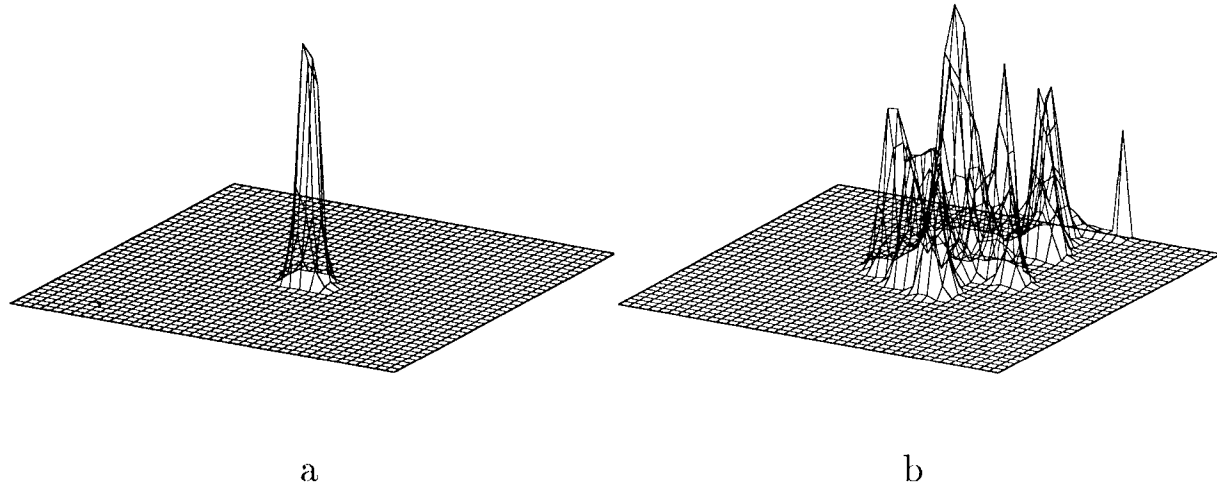


Fig. 2. Histogram of the tip position, (a) through the first 800 t.u., (b) through the whole duration of numerical experiment, 1.3×10^4 t.u. Medium size: 80×80 s.u. The peak at the far border of panel (b) corresponds to the tip attaching the boundary before dying out.

Eventually, we have chosen Barkley's model [16] for our experiments:

$$\partial u_1 / \partial t = \nabla^2 u_1 + \frac{1}{\epsilon} u_1 (1 - u_1) \left(u_1 - \frac{u_2 + b}{a} \right), \quad \partial u_2 / \partial t = u_1 - u_2 \quad (21)$$

for two reasons. First, it is the fastest for simulation, which is provided by the efficient numeric algorithm of [16]. This algorithm, in particular, includes resetting u_1 to the null-cline value 0 or 1 if it becomes too close (closer than $\delta = 10^{-3}$) to one of them, so that in a large number of nodes there is no need to compute Laplacian which is zero. Second, we were able to find parameter values which produced intensive and persistent hypermeander with clearly non-local tip trajectory:

$$a = 0.25, \quad b = 0.001, \quad \epsilon = 1/500. \quad (22)$$

Both these aspects are crucial, as the statistical predictions of Theorem 1 required very long experiments. The grid steps were chosen $h_x = 0.2$ s.u. in space and $h_t = 0.008$ t.u. in time. The time step is small enough to obey diffusion stability criterion $h_t < h_x^2/4$, but since $h_t/\epsilon = 4 > 1$, local kinetics of u_1 variable were calculated using implicit version of [16]. This choice of computation steps is rather far from giving a fully resolved PDE simulation – however, the major approximation error produced by the implicit calculation of fast local kinetics of u_1 did not influence the symmetry of the model, and change of the dynamic field in one time step always remained small. So, we believe that the computational model used is of a spatially extended dynamical system with all the required symmetry properties, and is suitable for testing the theory considered, no matter what is its exact relation to the PDE system (21).³

Maximal medium size was 80×80 s.u., i.e. 400×400 grid nodes. The spiral wave was initiated from cross-gradient initial conditions: u_1 was assigned to 0 in the left half of the medium and to 1 in the right half, and u_2 was assigned to 0 in the bottom half of the medium and to $a/2$ in the upper half. The spiral wave and typical tip trajectory are illustrated in Fig. 1.

This shows that the trajectory looks evidently more complicated than regular 'flowers' of simple meander, thus it may be called hypermeander. To see evolution of the tip at long times, we used histograms of tip position, obtained

³ In fact, computations with smaller steps give different behaviour (R. Mantel, private communication).

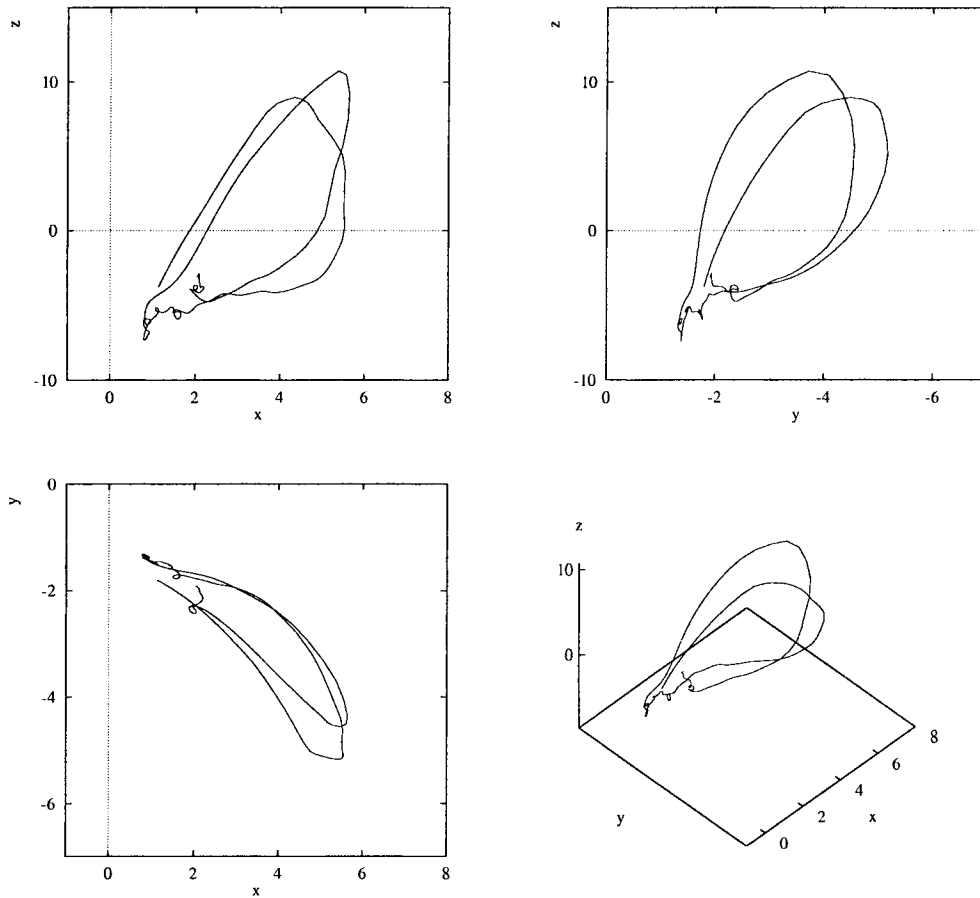


Fig. 3. A piece of trajectory of the quotient system (2) as extracted from the numerical experiment. Here the Cartesian coordinates x , y and z stand for c_x , c_y and ω of (2), respectively.

with bins of 5×5 grid cells (see Fig. 2). This solution was followed for about 1.65×10^6 time steps, or 1.3×10^4 t.u., when the spiral wave has died out by reaching the boundary.

It can be seen in that figure that the tip does walk in the plane to large distances. We have found that this trajectory is long enough to interpret the behaviour of this system in terms of the proposed theory.

To do that, we extracted tip path data $X(t)$, $Y(t)$ and $\Theta(t)$, where X and Y were coordinates of the crossing of two isolines,

$$u_1(X(t), Y(t), t) = 0.5, \quad u_2(X(t), Y(t), t) = 0.5a - b \quad (23)$$

and Θ was the azimuthal angle of ∇u_1 calculated at the tip point,

$$\Theta(t) = \arg[(\partial/\partial x + i\partial/\partial y)u_1(X(t), Y(t), t)]. \quad (24)$$

The gradient has been calculated by central differences at the corners of the computational cell containing the tip, and then bilinearly interpolated to the tip point.

The time derivatives dX/dt , dY/dt and $d\Theta/dt$ were substituted into (3) and (4) to reconstruct $c_{x,y}$ and ω . The numerical differentiation was performed with simplest Tikhonov regularisation procedure [17] with regularising

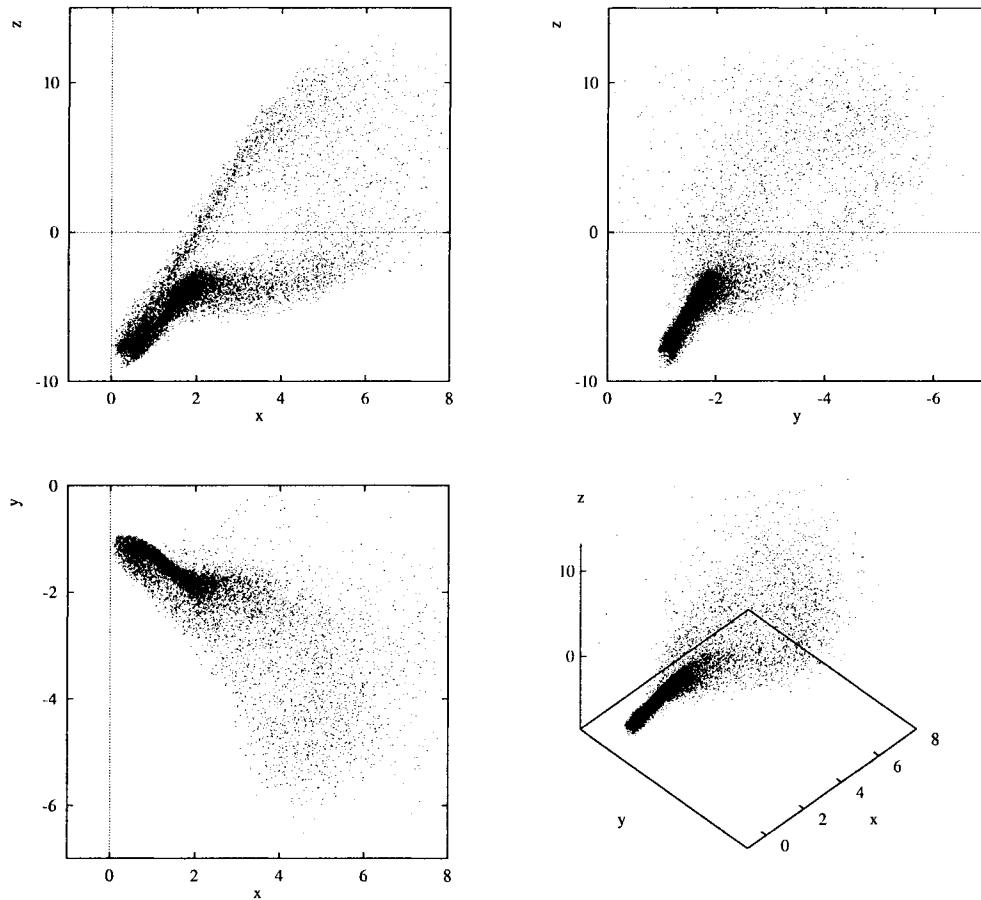


Fig. 4. Attractor of the system (2), i.e. a very long trajectory from the numerical experiment, shown by dots; coordinates are the same as in Fig. 3.

functional $\Lambda^2 \int (y')^2 dt$ equivalent to frequency filtering with window $1/(1 + (\Lambda\omega)^2)$, where the parameter Λ was chosen 0.06 t.u. The results are shown in Figs. 3–5.

Fig. 3 shows a typical projection of the trajectory in the quotient system in the axes (c_x, c_y, ω) . One loop typically consists of a large piece of a fast motion, corresponding to the quick jumps of the tip trajectory, and a smaller piece closer to the origin with a slower and oscillatory motion, corresponding to the sharp turns when the tip nearly stops. This shape of the trajectories in the quotient system is reminiscent of Shil'nikov chaos near a loop of a saddle-focus. Notice that this is close to the mechanism of transition to chaos via heteroclinic tangle hypothesised in [3,5] based on the Barkley's model system.

Fig. 4 shows the general look of the attractor in the quotient system, in the same coordinates. It is represented by about 12 000 points chosen equispaced with interval 10 t.s. or 0.08 t.u.

The accuracy of the computations is enough to see that it is a rather compact set – however, its fine structure is smeared out by the numerical noise.

Fig. 5 shows the attractor in the 'semi-reduced' system – same set of points in different coordinates (C_x, C_y, ω) . It looks clearly even in both x and y directions. Visually, its symmetry group may be \mathbf{Z}_4 or $\mathbf{SO}(2)$; the latter is more likely as the \mathbf{Z}_4 -shape of the central hole of the top view should probably be attributed to the influence of the square grid, which is naturally more noticeable at low propagation speeds.

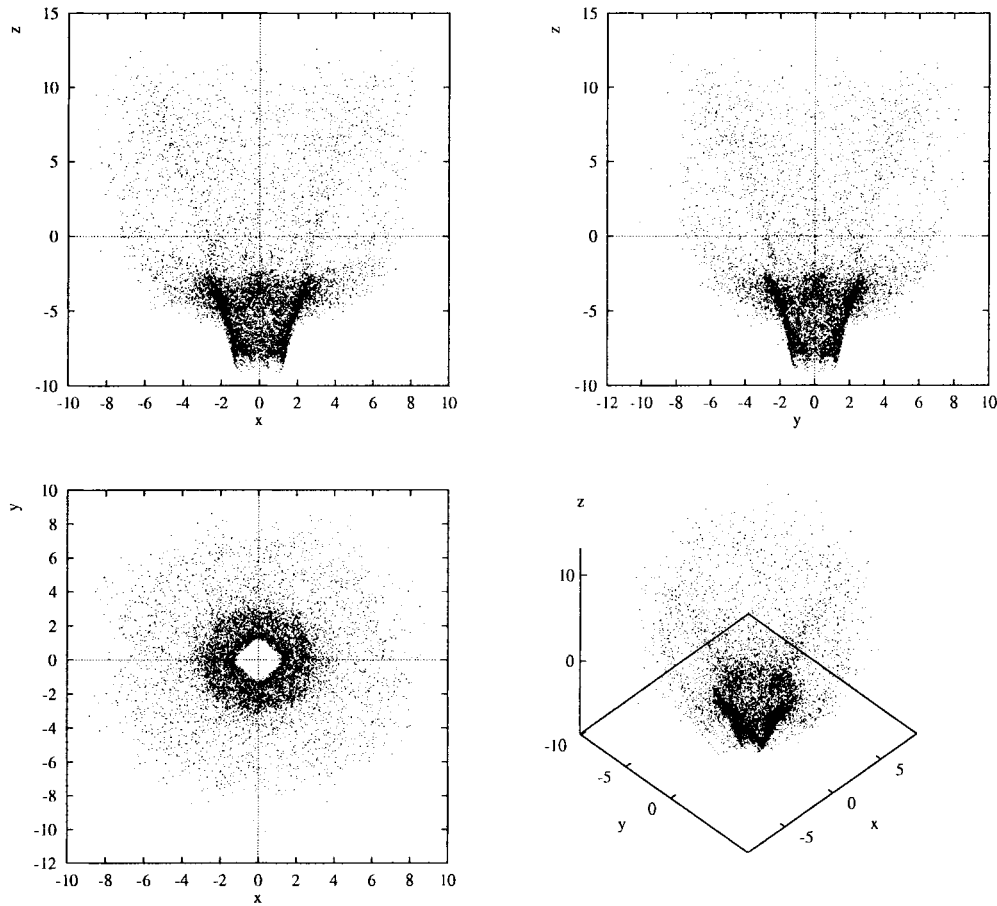


Fig. 5. Attractor in the semi-reduced system extracted from numerical experiment, with x , y denoting tip velocity components C_x and C_y , and z still being ω .

At any rate, the parity of the attractor in the semi-reduced system means that the large-time behaviour should be of Brownian type without directed component. To check this, we measured directly the mean squared walking distance as a function of time (Fig. 6).

We assumed ergodicity and calculated the mean squared walking distance by splitting the trajectory from the longest experiment onto pieces of equal length and averaging the square of distance between the ends of each piece. The resulting dependence is shown by dots in Fig. 6 (about 3000 points).

Leftmost part of the graph, for $t < 0.5$ t.u., with slope 2 represents differentiability of the trajectories. The range 0.5–10 t.u. is characteristic time range of the attractor in the quotient system. At the times larger than 10 t.u., growth of the displacement due to diffusive motion is seen up to times 2000 t.u. when averaging time intervals become comparable to the length of the experiment, and ergodicity fails.

The long-time walking distance is significantly larger than the typical size of one meandering petal, and so approximations (20) may be sensible in the scale between 10 and 2000 t.u. We fitted the data to (20) and to a more generic dependence

$$I(t) \approx 2K_0 t^\alpha + 2K_1 \quad (25)$$

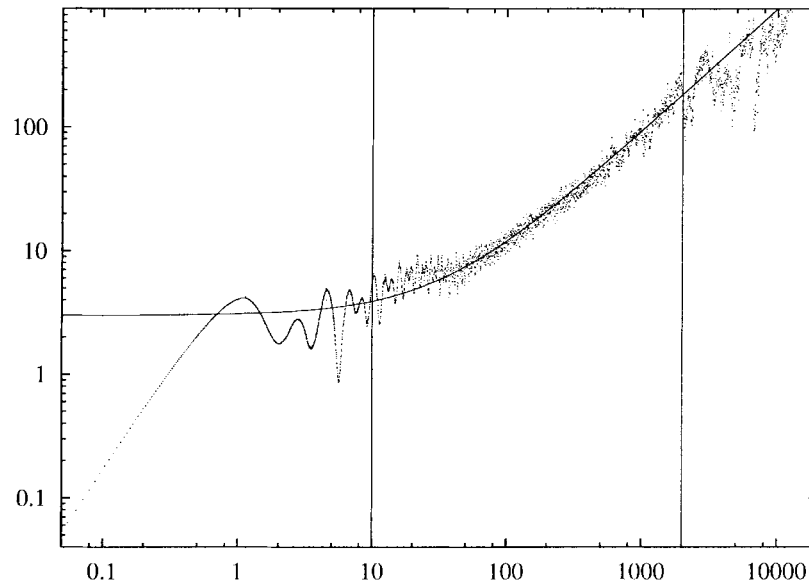


Fig. 6. Mean square of the displacement of the tip $I(t)$ vs. time t (dots), and fitting curve (solid line) in logarithmic coordinates. Vertical lines show the fitting range.

in logarithmic coordinates, using Marquard's method [18] with equal weights of all points (about 5000) in the range 10–2000 t.u., i.e. more than two decades. Fitting by (20) yielded coefficients $2K_0 \approx 0.090$ and $2K_1 \approx 2.99$, and good agreement with the experimental data in two decades of t (see Fig. 6). The reliability of this approximation can be seen from fitting the same data to (25), which yielded $\alpha = 1.09 \pm 0.03$. Thus, the experimental dependence of $I(t)$ in a proper range of t is reasonably approximated by (20), with the hypermeandering diffusion coefficient $K_0/2 \approx 0.023$, i.e. 40 times less than the diffusion coefficient of the propagator variable. So, the hypermeander diffusion is rather intensive and hardly can be attributed to the numerical noise.

4. Discussion

In this paper, we have described the simplest mathematical features of continuous deterministic Brownian motion, i.e. unlimited walk driven by deterministic chaotic force, and have shown that the complicated patterns of spiral wave meandering observed in numerical experiments may be interpreted as such a motion.

This sort of motion results from two main features of the mathematical problem. The first is the difference between symmetry groups of the dynamical system and particular solutions, so that the factor group, if it is non-compact, gives birth to a non-compact set of congruent solutions and thus creates the possibility of unlimited drift along this set. The other is chaos in the quotient systems, which makes this drift similar to stochastic Brownian motion. We have considered the case of continuous factor group, and predicted two types of deterministic Brownian motion, with or without directed component. Which type occurs in a particular case depends on whether or not the maximal attractor of the semi-reduced system is uniquely ergodic.

Non-symmetric solutions of symmetric systems are ubiquitous, and in all such cases, non-compact factor group and chaotic dynamics in the quotient system can lead to deterministic Brownian motion or deterministic diffusion. Theorem 1 describes such a motion in case when the factor group is the group of translations of the straight line, as in [11]. The hypermeander of spiral waves considered in this paper is a more complicated motion as the

symmetry group involved, $\mathbf{SE}(2)$, is non-commutative, the corresponding three-dimensional manifold is curved and Theorem 1 is not applicable directly. We were able to overcome this difficulty by noting that $\mathbf{SE}(2)$ can be decomposed onto two Abelian subgroups, those of translations and rotations, and reduction by the subgroup of translations yields the required result. Deterministic chaos-driven walk along more complicated groups presents an interesting mathematical problem for future study.

Acknowledgements

We are grateful to Profs. P. Coullet and A. Winfree and Drs. P. Ashwin, D. Barkley and E. Nikolaev for fruitful and encouraging discussions, and to I. Biktasheva for help in processing the results of numerical experiments. Special thanks to Prof. E. Shnol who has read the manuscript and suggested several corrections and improvements. This work was supported in part by grants from The Wellcome Trust (045192), EPSRC ANM (448838) and Russian Fund for Basic Research (96-01-00592).

Appendix A. Proof of Theorem 1

Due to ergodicity of μ , averaging over time and in μ are equivalent, and it is enough to prove the statements of the theorem for the μ -averaged squared distance:

$$\tilde{I}_\mu(t) = \int (q(t, u) - q(0, u))^2 d\mu(u), \quad (\text{A.1})$$

which equals $I(t, u)$ for almost all u with respect to μ .

Straightforward calculations give

$$\tilde{I}_\mu(t) = \int d\mu(u) \left(\int_0^t V(F^\tau(u)) d\tau \right) \left(\int_0^t V(F^\sigma(u)) d\sigma \right) \quad (\text{definition of } q(t)) \quad (\text{A.2})$$

$$= \int_0^t d\tau \int_0^t d\sigma \left(\int V(F^\tau(u)) V(F^\sigma(u)) d\mu(u) \right) \quad (\text{change of order of integration}) \quad (\text{A.3})$$

$$= \int_0^t \int_0^t K(\tau - \sigma) d\tau d\sigma \quad (\text{definition of } K(\tau)) \quad (\text{A.4})$$

$$= 2 \int_0^t d\xi \int_0^\xi K(\eta) d\eta \quad (\text{change of independent variables, } \tau + \sigma = \xi, \tau - \sigma = \eta) \quad (\text{A.5})$$

$$= K_0 t - 2 \int_0^t d\xi \int_\xi^{+\infty} K(\eta) d\eta \quad (\text{definition of } K_0) \quad (\text{A.6})$$

$$= K_0 t + \int_0^t o(1)|_{\xi \rightarrow \infty} d\xi \quad (\text{convergence of } K_0). \quad (\text{A.7})$$

$$= K_0 t + o(t)|_{t \rightarrow \infty} \quad (\text{L'Hospital's rule}). \quad (\text{A.8})$$

The last estimation is the statement (9) of the theorem.

Analogously, using (10) in (A.7) in addition to (7) leads to a more accurate estimation (11).

References

- [1] V.N. Biktashev, A.V. Holden, E.V. Nikolaev, Spiral wave meander and symmetry of the plane, *Int. J. Bifurc. & Chaos* 6 (12) (1996) 2433–2440.
- [2] D.V. Anosov, V.I. Arnold (Eds.), *Dynamical Systems I*, Springer, Berlin, 1985, p. 31.
- [3] D. Barkley, I.G. Kevrekidis, A dynamical systems approach to spiral wave dynamics, *Chaos* 4 (3) (1994) 453–460.
- [4] D. Barkley, Euclidean symmetry and the dynamics of rotating spiral waves, *Phys. Rev. Lett.* 72 (1994) 164–167.
- [5] D. Barkley, Spiral meandering, in: R. Kapral, K. Showalter (Eds.), *Chemical Waves and Patterns*, Kluwer, Academic Publishers, Dordrecht, 1995.
- [6] C. Wulff, Bifurcation theory of meandering spiral waves, in: Z. Parisi, S.C. Müller, W. Zimmermann (Eds.), *Nonlinear Physics of Complex Systems – Current Status and Future Trends*, Springer, Berlin, 1996.
- [7] A.T. Winfree, Varieties of spiral wave behaviour – an experimentalist’s approach to the theory of excitable media, *Chaos* 1 (1991) 303–334.
- [8] W. Jahnke, A. Winfree, A survey of spiral-wave behaviors in the Oregonator model, *Int. J. Bifurc. & Chaos* 1 (2) (1991) 445–466.
- [9] C. Diks, B. Hoekstra, J. DeGoede, Spiral wave dynamics, *Chaos Solitons and Fractals* 5 (3/4) (1995) 645–660.
- [10] T. Geisel, J. Nierwetberg, Universal fine-structure of the chaotic region in period-doubling systems, *Phys. Rev. Lett.* 47 (14) (1981) 975–978.
- [11] P. Coullet, K. Emilsson, Chaotically induced defect diffusion, in: E. Tirapegui, W. Zeller (Eds.), *Instabilities and Nonequilibrium Structures V*, Kluwer, Academic Publishers, Dordrecht, 1996, pp. 55–62.
- [12] E.V. Nikolaev, Bifurcations of limit cycles of differential equations possessing a finite symmetry group, (in Russian), Ph.D. Thesis, State University of Nizhny Novgorod, 1995.
- [13] R.M. Mantel, D. Barkley, Periodic forcing of spiral waves in excitable media, *Phys. Rev. E* 54 (5) (1996) 4791–4802.
- [14] R. Jones, W. Parry, Compact Abelian group extensions of dynamical systems II, *Comp. Math.* 25 (2) (1972) 135–147.
- [15] T. Plesser, K.H. Müller, Fourier analysis of the complex motion of spiral tips in excitable media, *Int. J. Bifurc. & Chaos* 5 (4) (1995) 1071–1084.
- [16] D. Barkley, A model for fast computer simulation of waves in excitable media, *Physica D* 49 (1991) 61–70.
- [17] N.S. Bakhvalov, *Numerical Methods (Algebra, Analysis, Ordinary Differential Equations)* (in Russian), Nauka, Moscow, 1973.
- [18] W.H. Press, S.A. Teukolsky, W.T. Vetterling, B.P. Flannery, *Numerical Recipes, The Art of Scientific Computing*, Cambridge University Press, Cambridge, 1992.